Geophysical Research Letters

RESEARCH LETTER
10.1029/2018GL081805

Melting of $CaSiO_3$ Perovskite at High Pressure

James Braithwaite[1] and Lars Stixrude[1,2]

[1]Department of Earth Sciences, University College London, London, UK, [2]Now at Department of Earth, Planetary, and Space Sciences, University of California, Los Angeles, CA, USA

Key Points:
- Calcium silicate perovskite melts at 5600 K at the core mantle boundary
- Metasilicate liquids are denser than coexisting crystalline silicates at the core-mantle boundary
- The Z method allows precise ab initio melting temperature determination

Supporting Information:
- Supporting Information S1

Correspondence to:
L. Stixrude,
lstixrude@epss.ucla.edu

Citation:
Braithwaite, J., & Stixrude, L. (2019). Melting of $CaSiO_3$ perovskite at high pressure. *Geophysical Research Letters*, *46*, 2037–2044. https://doi.org/10.1029/2018GL081805

Received 29 DEC 2018
Accepted 9 FEB 2019
Accepted article online 13 FEB 2019
Published online 21 FEB 2019

Abstract Ab initio molecular dynamics simulations predict that $CaSiO_3$ perovskite melts at 5600 K at 136 GPa, and 6400 K at 300 GPa, significantly higher than $MgSiO_3$ perovskite. The entropy of melting (1.8 k_B per atom) is much larger than that of many silicates at ambient pressure and of simple liquids and varies little with pressure. The volume of melting decreases rapidly with increasing pressure, to 3 % at 136 GPa, producing a melting slope that diminishes rapidly with pressure. We determine the melting temperature via the ZW method, combining the Z method, for which we clarify the theoretical basis, with a waiting time analysis. The ZW method results are internally confirmed by integrating the Clausius-Clapeyron equation, which also yields our results for the entropy and volume of melting. We find the eutectic composition on the $MgSiO_3$-$CaSiO_3$ join to be $x_{Ca} = 0.26$ at 136 GPa and that metasilicate melt is denser than coexisting silicates.

Plain Language Summary Silicate melting is a major agent of thermal and chemical evolution of the Earth and other rocky planets. The melting temperature of Calcium silicate perovskite, a mineral that exists in Earth's lower mantle, is unknown over most of the pressure range that occurs in the mantle of Earth and super-Earth exoplanets. We use advanced quantum mechanical simulations to predict the melting temperature of this material. We find that the melting temperature increases with increasing pressure but at a rate that diminishes continuously. The liquid and crystal have very similar volumes in the deep portions of planetary mantles, supporting the view that crystals may float at great depth.

1. Introduction

$CaSiO_3$ perovskite is the third most abundant phase in Earth's lower mantle. This phase may have played an important role in the evolution of the magma ocean as it is denser than bulk silicate Earth compositions and would be expected to sink as it crystallized, carrying with it much of Earth's complement of radioactive heat producing elements, as well as important geochemical tracers, such as Nd and Sm (Corgne et al., 2005; Tateno et al., 2018).

However, the melting temperature of $CaSiO_3$ perovskite is unknown over most of Earth's pressure range. Experimental measurements exist only up to 58 GPa, and at the upper end of this range, there is significant disagreement among different experiments (Shen & Lazor, 1995; Zerr et al., 1997). In whole rock compositions, experiments show that $CaSiO_3$ perovskite is the solidus phase in peridiotite up to 60 GPa, and at higher pressure crystallizes second, after bridgmanite (Fiquet et al., 2010). In basaltic compositions, $CaSiO_3$ perovksite is the liquidus phase throughout the lower mantle regime (Tateno et al., 2018).

Because of its simple crystal structure (cubic, five atoms per unit cell) and wide stability field (14–600 GPa; Gasparik et al., 1994; Tsuchiya & Tsuchiya, 2011), $CaSiO_3$ perovskite is an ideal system to test theoretical methods for predicting the melting temperature. It also provides a point of comparison with the melting of Earth's most abundant phase Mg-rich silicate perovskite (bridgmanite), the melting of which has been more widely studied. Melting of $CaSiO_3$ has not previously been studied with first-principles methods. Computing the melting temperature theoretically is challenging, because it requires either knowledge of the free energy, which is not available from standard molecular dynamics simulations, or a dynamical method of converting one phase to another.

Here we determine the melting temperature of $CaSiO_3$ perovksite with the ZW method, which allows one to extract the equilibrium melting temperature from an analysis of homogeneous melting. In order to test internally our ZW method results, and to gain more insight into the melting process, we also compute the melting

temperature via integration of the Clausius-Clapeyron equation. The combination allows us to determine not only the melting temperature but also the volume and entropy of melting.

2. Theory

The melting process in infinite, periodic, surface-free systems, such as ours, is referred to as homogeneous melting. This process differs from that studied experimentally where nucleation sites, provided by sample containers and grain-grain contacts, are typically abundant. The homogeneous melting point is always greater than the equilibrium melting temperature. Homogeneous melting can be studied experimentally with special design of sample containers or energy input (Daeges et al., 1986; Mo et al., 2018).

Consider a homogeneous solid in the microcanonical ensemble: with fixed particle number N, volume V, and internal energy E. As we increase the energy, we find that solid and liquid coexist in thermodynamic equilibrium over a range of energies from E_M, the largest energy at which pure solid is stable, to E_H, the smallest energy at which pure liquid is stable. In a homogeneous system, solid-liquid coexistence is not possible: The solid is retained until the energy at which liquid is first stable as a homogeneous phase: E_H. This energy corresponds to a temperature T_H: the homogeneous melting temperature, which represents the limit of superheating of the solid. As the solid melts at constant $E = E_H$, the temperature drops, due to the latent heat of melting, to a new temperature T_M: the equilibrium melting temperature

$$E_H = E^{\text{solid}}(V, T_H) = E^{\text{liquid}}(V, T_M). \tag{1}$$

The goal of the Z method is then to locate the energy E_H above which the solid always transforms to the liquid (Belonoshko et al., 2006; Gonzalez-Cataldo et al., 2016).

To see the relationship between the homogeneous and equilibrium melting temperatures in the microcanonical ensemble, assume the energy of the solid varies linearly with temperature near T_M, yielding

$$T^{-1} \equiv \left(\frac{\partial S}{\partial E}\right)_{V,N} = \left[T_M + (E - E_M)/C_V\right]^{-1}, \tag{2}$$

where C_V is the heat capacity and the first relationship is the definition of temperature. Integrating

$$S = S_M + C_V \ln\left(\frac{E - E_M}{C_V T_M} + 1\right), \tag{3}$$

which increases monotonically with increasing energy. The entropy constitutes the fundamental thermodynamic relation, in the sense of Callen (1960), along the isochore and is most useful for visualizing the homogeneous melting process, as the stable state is the one with the greatest entropy. We find the temperature of homogeneous melting by taking the derivative with respect to energy and evaluating at the energy where the liquid first becomes thermodynamically stable as a homogeneous phase $E = E_M + \Delta E_M$ where ΔE_M is the energy of melting

$$T_H^{-1} = \left.\frac{\partial S}{\partial E}\right|_{E=E_M+\Delta E_M} = \frac{\Delta E_M + C_V T_M}{C_V}, \tag{4}$$

which can also be obtained by subsituting for the energy in equation (2). Rearranging and using $\Delta E_M = T_M \Delta S_M$ where ΔS_M is the entropy of melting

$$T_H/T_M - 1 = \Delta S_M/C_V \tag{5}$$

and we have neglected only the influence of pressure on the equilibrium melting temperature on the interval $[P(V, E_M), P(V, E_H)]$. We expect the ratio on the right-hand side of equation (5) to vary slowly with pressure, because ΔS and C_V vary slowly with pressure. An identical equation was derived by Belonoshko et al. (2006) on heuristic grounds.

An example illustrates these relationships (Figure 1). For the purposes of this illustration of the method, we focus on the melting of $MgSiO_3$ bridgmanite at $\rho = 5$ g/cm^3, with the properties of bridgmanite from HeFESTo (Stixrude & Lithgow-Bertelloni, 2011) and those of $MgSiO_3$ liquid from our previous simulation

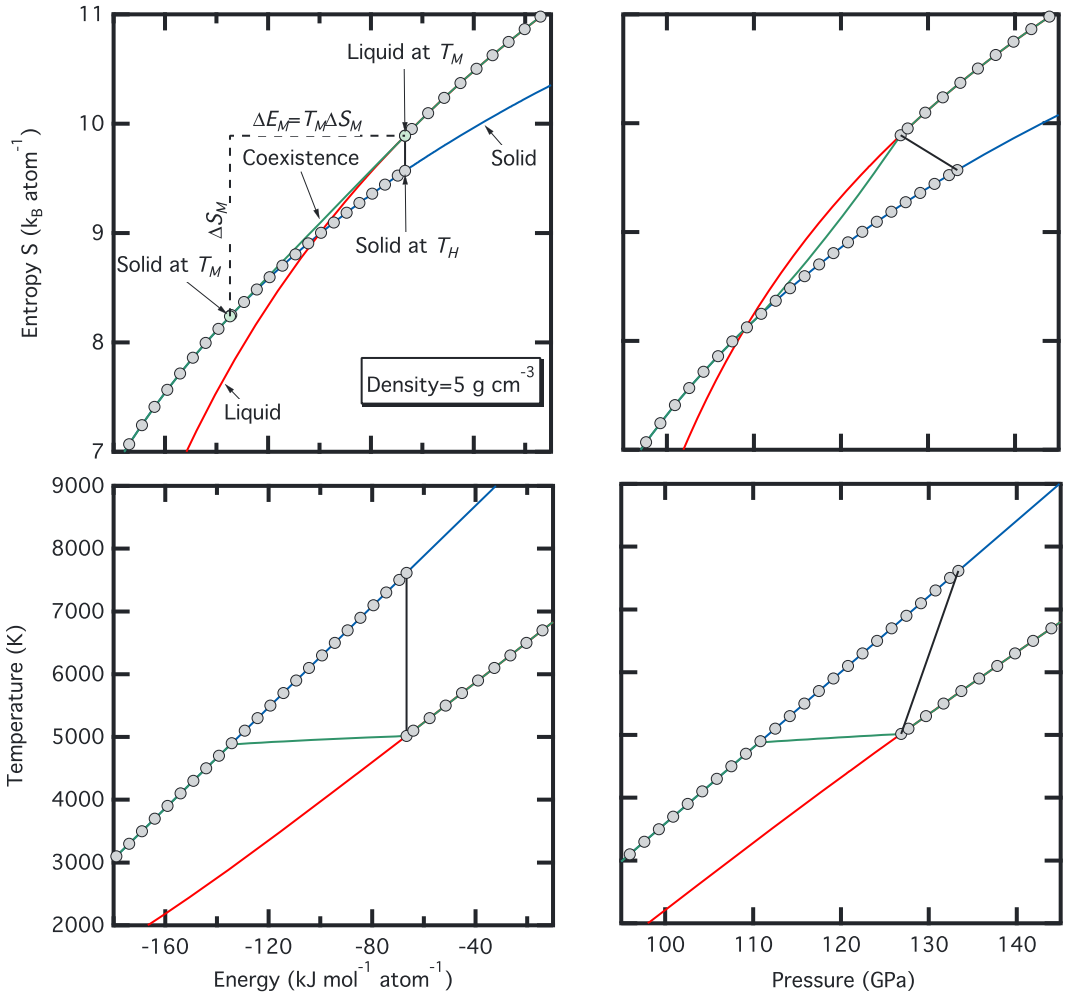

Figure 1. Illustration of the Z method using our results for $MgSiO_3$ (de Koker & Stixrude, 2009). Thermodynamic paths along the 5 g/cm^3 isochore of pure liquid (red), pure solid (blue), equilibrium coexistence of the two phases (green), and homogeneous melting (gray circles and black line) in entropy, energy, temperature, and pressure space. The green circles in the top left figure represent, at lower energy, the energy at which the solid first begins to melt and, at higher energy, the energy at which melting ends and the liquid first becomes thermodynamically stable as a homogeneous phase on heating. The difference in entropy and energy between these two green points are the entropy ΔS_M and energy $\Delta E_M = T_M \Delta S_M$ of melting, respectively.

studies (de Koker & Stixrude, 2009). The figure shows an important point that is not widely recognized: While the solid to liquid portion of the Z trajectory is generally assumed to have a negative slope in pressure-temperature space, for our example, the slope is positive. The slope reflects the relative magnitudes of the pressure increase along the solid isochore between T_M and T_H versus the increase in pressure due to melting. The latter decreases with increasing pressure as the volume of melting decreases, leading to a positive slope at high pressure.

In practice, the Z method can only provide an upper bound to the equilibrium melting temperature T_M (Alfe et al., 2011). The reason is that as we approach E_H from above, the waiting time τ_W required for the solid to transform to liquid diverges. We estimate the melting temperature by measuring τ_W from our simulations as a function of liquid state temperature and extrapolating to the limit of infinite waiting time. In order to measure τ_W, we compute at each time step the amplitude of the peak in the structure factor $S(\mathbf{q}) = 1/N \sum_{j,k}^{N} \exp\left[-i\mathbf{q} \cdot (\mathbf{r}_k - \mathbf{r}_j)\right]$ with $\mathbf{q} = (2,0,0)2\pi/a$, and a the primitive lattice constant, and find the time at which the amplitude drops, typically a factor of 2 or more on melting. We refer to the augmentation of the Z method with the waiting time analysis as the ZW method.

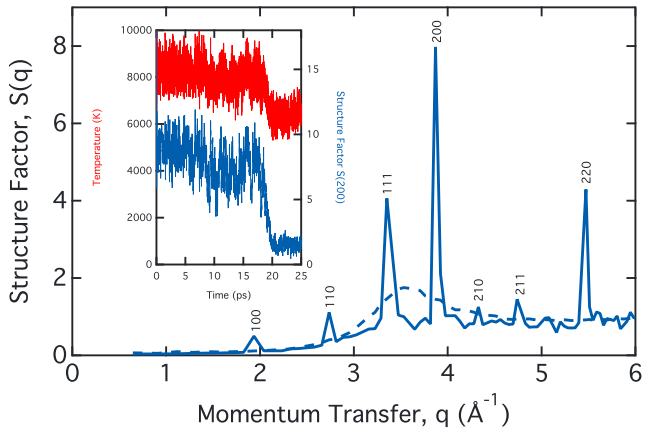

Figure 2. Results of a microcanonical simulation at $V = 4.12$ cm^3·mol^{-1}·atom^{-1} showing (inset) the temperature (red) and the amplitude of the (200) peak in the structure factor (blue) as a function of time. The main figure shows the structure factor averaged over the crystalline (first 15 ps, solid line) and liquid (last 5 ps, dashed line) portions of the trajectory. The drop in temperature and structure factor amplitude near 18 ps is due to the crystal to liquid transition.

We have also computed the melting curve via an independent method based on integration of the Clausius-Clapeyron equation, following our previous work (de Koker & Stixrude, 2009; Stixrude & Karki, 2005)

$$T_M = T_{M0} \exp\left[\int_{P_0}^{P} \frac{\Delta V}{\Delta H} \mathrm{d}P'\right], \tag{6}$$

where ΔV and ΔH are, respectively, the volume and enthalpy of melting. This approach requires one assumed fixed point along the melting curve (indicated by the subscript 0), which we take to be the lowest pressure point from the ZW method.

Our simulations are based on density functional theory in the PBEsol approximation to the exchange-correlation functional (Perdew et al., 2008) and the projector augmented wave (PAW) method (Kresse & Joubert, 1999) as implemented in VASP (Kresse & Furthmuller, 1996). We use PAW potentials with, respectively, for Ca, Si, and O: 10, 4, and 6 valence electrons and core radii of 1.22, 1.01, and 0.80 Å. We assume a basis set size given by an energy cutoff of 500 eV and Brillouin zone sampling at the Gamma point only, which leads to convergence of energy and pressure to within 7 meV per atom and 0.3 GPa. We assume thermal equilibrium between ions and electrons via the Mermin functional (Mermin, 1965; Wentzcovitch et al., 1992).

All of our results are based on a simulation cell with $N = 135$ ($3 \times 3 \times 3$ supercell). The cell shape is cubic corresponding to the symmetry of the stable crystalline perovksite structure at high temperature (Stixrude et al., 2007). We perform Z method calculations in the microcanonical ensemble. The initial configuration is the perfect lattice, and we add energy by assigning initial velocities drawn from a Maxwell-Boltzmann distribution. We run the simulations for at least 5 ps, and much longer in the vicinity of E_H, up to 30 ps. We determine the equations of state of liquid and solid phases in the canonical ensemble (constants N, V, and T) with the temperature controlled by the Nosé-Hoover thermostat (Hoover, 1985). We assume a time step of 1 fs for all simulations.

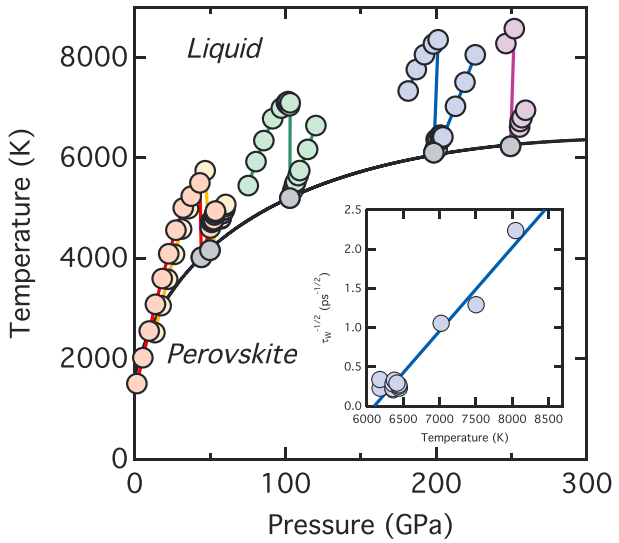

Figure 3. Results of microcanonical simulations along the isochores: 5.80 (red), 5.74 (orange), 4.91 (green), 4.12 (blue), and 3.85 (purple) cm^3·mol^{-1}·atom^{-1}. The gray circles indicate the results of the waiting time analysis along each isochore. The black line is a fit to the waiting time results (Kechin, 2002): $T_M(P) = T_0(1 + \frac{P-P_0}{a})^b \exp(-\frac{P-P_0}{c})$, with $T_0 = 4020$ K, $P_0 = 44.2$ GPa, $a = 48.8$ GPa, $b = 0.413$, and $c = 860$ GPa. The inset shows an example of the waiting time analysis at 4.12 cm^3·mol^{-1}·atom^{-1}.

3. Results

The Z method allows us precisely to define the conditions of homogeneous melting (Figure 2). The temperature and structure factor show clear signals upon the transition from crystallline to liquid states: In the example shown, the temperature drops by 1600 K, and the amplitude of the (200) peak in the structure factor drops by a factor of 5 over a time interval of a few picoseconds. The structure factor over the crystalline portion of the trajectory shows all peaks expected of the cubic perovksite structure, confirming that the structure remains stable up until the homogeneous melting transition.

As expected our results show nearly linear isochoric paths in pressure-temperature space for both crystalline and liquid phases (Figure 3). Slight curvature in the solid isochores near T_H reflects anharmonicity at superliquidus temperatures. The maximum temperature attained is the homogeneous melting temperature T_H, which increases monotonically on compression. The lowest temperature along the liquid portion of the isochore also rises monotonically on compression and is an upper bound to the equilibrium melting temperature T_M.

To determine the equilibrium melting temperature T_M, we analyze the waiting time to melting (Figure 3 and Table S1 in the supporting information). We find that the dependence of τ_W on the liquid state temperature

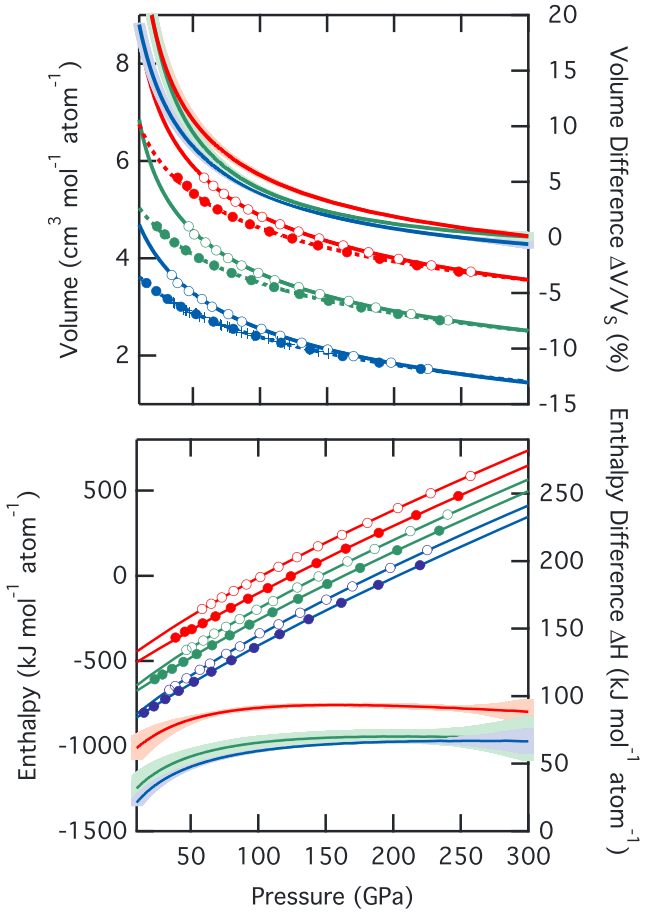

Figure 4. Results of canonical simulations along the 2000- (blue), 4000- (green), and 6000-K (red) isotherms shown as open (liquid) and filled (solid) symbols. The volume (top) and enthalpy (bottom) are plotted against the left-hand axis, while the liquid-solid differences are plotted against the right-hand axis as indicated and the volume of melting is expressed as $\Delta V/V_S$ where V_S is the volume of the solid phase. The envelopes about the curves corresponding to ΔH and $\Delta V/V_S$ indicate propagated uncertainties. For clarity the volumes at 4000 and 2000 K are shifted downward by 1 and 2 cm^3/mol, respectively, and the enthalpies at 4000 and 2000 K are shifted downward by 100 and 200 kJ/mol, respectively. Shown for comparison are the experimental measurements of the volume of $CaSiO_3$ perovksite along the 2000-K isotherm (blue plus symbols; Sun et al., 2016).

T_L is well approximated by the form proposed by Alfe et al. (2011):

$$\tau_W^{-1/2} = A(T_L - T_M) \tag{7}$$

so that T_M is found as the intercept of this relation at $\tau_W^{-1/2} = 0$. The equilibrium melting temperature increases monotonically with increasing pressure. The melting slope decreases with increasing pressure and remains positive up to the highest pressure of our study. We find that the ratio $T_H/T_M - 1$ is nearly independent of pressure (Table S1) as our analysis (equation (5)) predicts.

Our canonical simulations show that the liquid-solid volume contrast decreases with increasing pressure but remains positive throughout the pressure range of our simulations (Figure 4). At the conditions of Earth's core-mantle boundary, the liquid-solid volume contrast $\Delta V = 2.8\%$, very similar to the value found in the $MgSiO_3$ and $CaMgSi_2O_6$ systems at the same conditions (Stixrude & Karki, 2005; Sun et al., 2011). The liquid-solid enthalpy contrast ΔH is everywhere greater than 0, reflecting the latent heat of melting. With increasing temperature, ΔV and ΔH increase, reflecting the greater thermal expansivity and heat capacity, respectively, of the liquid phase as compared with the solid phase.

The melting curve computed from the Clausius-Clapeyron equation agrees well with that obtained from the ZW method (Figure 5). We integrated equation (6) with $P_0 = 44.2$ GPa and $T_0 = 4020$ K from our lowest pressure ZW method result. We compare integrations using values of $\Delta V/\Delta H$ taken from the three different

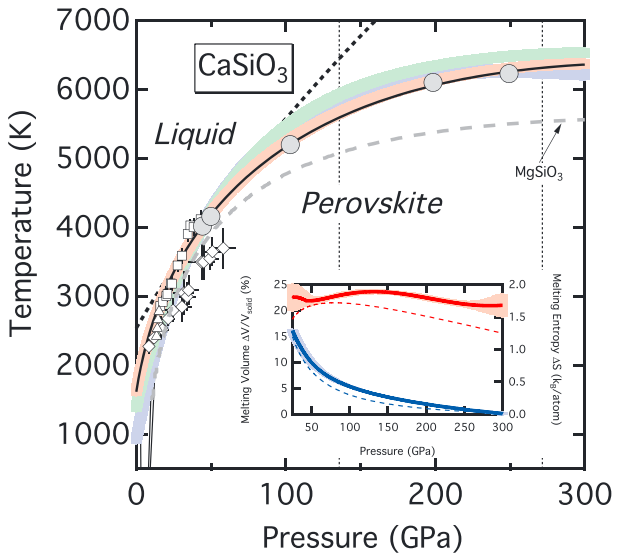

Figure 5. Results of the Clausius-Clapeyron integration shown by the envelopes computed from $\Delta V/\Delta H$ at 2000 (blue), 4000 (green), and 6000 K (red) compared with the results of the ZW method (gray circles) and the best fitting curve (black line, same as in Figure 3). For comparison we show the $MgSiO_3$ melting curve from de Koker and Stixrude (2009; long gray dashed line), the Lindeman melting curve (bold short dashed line), and the solid-solid phase transformations from wollastonite to walstromite to larnite + $CaSi_2O_5$ titanite (thin solid lines). Experimental measurements of melting are from Gasparik et al. (1994; triangles), Shen and Lazor (1995; diamonds), and Zerr et al. (1997; squares). Vertical dotted lines show the pressure at the core-mantle boundary of Earth and that of a 2 Earth-mass super-Earth of the same composition (Stixrude, 2014). The inset shows the volume (blue) and entropy (red) of melting along the computed melting curve. For comparison we show as dashed lines the corresponding results for $MgSiO_3$ (de Koker et al., 2013).

isotherms of our simulations (2000, 4000, and 6000 K; Figure 4). The close agreement among these three integration results shows that $\Delta V/\Delta H$ is nearly independent of temperature as previously found for alkali halides (Boehler et al., 1996). We interpolate our results for ΔV and ΔH in order to obtain the volume and enthalpy of melting and compute the entropy of melting as $\Delta S = \Delta H/T_M$. The volume of melting decreases rapidly with increasing pressure, although it does not vanish until the high pressure limit of our results. The entropy of melting is nearly invariant with pressure, and much larger than that of many silicate at ambient conditions and of simple liquids, which show $\Delta S \sim 1.0\ k_B$ per atom (Stebbins et al., 1984). The entropy of melting of $MgSiO_3$ perovskite also substantially exceeds $1.0\ k_B$ per atom, which we have attributed to the larger range of coordination environments in the liquid at high pressure, as compared with that at low pressure, where the liquid is almost completely fourfold Si-O coordinated (Stixrude et al., 2009).

4. Discussion

We find excellent agreement between our computed melting curve and experimental data at the low pressure limit of perovskite stability where multiple experiments are mutually consistent (Figure 5). At higher pressures, measurements from different experiments diverge. Our results are consistent with the measurements of Zerr et al. (1997) but deviate significantly from those of Shen and Lazor (1995) at the highest pressures of their experiments. The melting temperature of $CaSiO_3$ perovskite is significantly higher than that of $MgSiO_3$ perovskite and increases more rapidly with pressure. The greater slope of the $CaSiO_3$ melting slope can be understood on the basis of the Clausius-Clapeyron relation $\partial T_M/\partial P = \Delta V/\Delta S$ and is due to the larger volume of melting in the Ca end-member.

The volume of fusion decreases rapidly with increasing pressure and approaches 0 at the highest pressures of our study (Figure 5). This rapid decrease has two important consequences. The first is that the melting slope $\partial T_M/\partial P$ diminishes rapidly with increasing pressure: The melting temperature is nearly independent of pressure at the highest pressure of our study. The pronounced curvature of the melting line differs markedly from the predictions of the Lindemann law:

$$T_{\text{Lindemann}} = f^2 \frac{\bar{m} k_B \bar{v}^{2/3} \theta^2}{9\hbar^2}, \tag{8}$$

where $\bar{m}$ and $\bar{v}$ are the mean atomic mass and volume, respectively, $\hbar$ is the Planck constant divided by 2π, θ is the Debye temperature, which we take from our thermodynamic model (Stixrude & Lithgow-Bertelloni, 2011), and f is the critical ratio of vibrational amplitude to interatomic spacing at melting, which we set so that our lowest pressure ZW method result is reproduced, yielding $f = 0.137$. The Lindemann melting curve is much steeper than ours and much less curved (Figure 5). This is due to the one-phase nature of the Lindemann criterion, which neglects structural change in the liquid (Hoover & Ross, 1971). All silicate liquids undergo pronounced structural change over the mantle pressure regime (Stixrude et al., 2009) including $CaSiO_3$ liquid (Bajgain et al., 2015), causing them to compress more efficiently than an isostructural liquid, and the melting slope to decrease more rapidly than the Lindemann prediction. The second important consequence of the small volume of fusion at the base of the mantle is that the volume of fusion no longer governs crystal-liquid buoyancy, which is instead controlled by element partitioning, particularly of relatively abundant, heavy, and incompatible elements, such as Ca and Fe (Stixrude & Karki, 2005).

We use our results to estimate eutectic melting on the $MgSiO_3$-$CaSiO_3$ join. We assume ideal mixing in the liquid phase, no solid solution between the two perovskite phases, and neglect the temperature dependence of the liquid-crystal entropy contrast, yielding, for the liquidus temperature T_α in equilbrium with a solid of

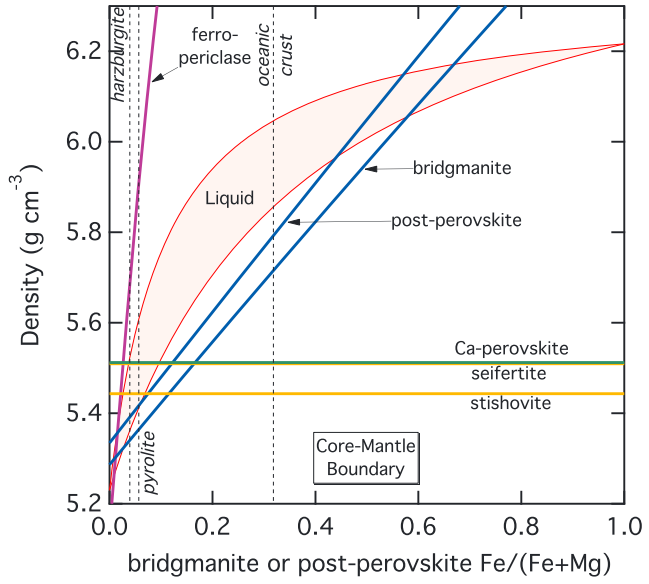

Figure 6. The density of liquid as a function of the Fe content of coexisting bridgmanite or postperovskite assuming values of $K_D = 0.1$ (Tateno et al., 2014; upper bound) and K_D=0.3 (Andrault et al., 2012; lower bound) compared with that of lower mantle phases as computed with HeFESTo (Stixrude & Lithgow-Bertelloni, 2011) at 135.8 GPa and 4000 K. Vertical dashed lines indicate the value of x_{Fe} of bridgmanite as computed with HeFESTo in the indicated lithologies, the bulk compositions of which are specified in Xu et al. (2008).

pure component α, which melts at $T_{\alpha 0}$

$$T_\alpha = T_{\alpha 0}\left(1 - \frac{R}{\Delta S_{\alpha 0}} \ln x_\alpha\right)^{-1}, \quad (9)$$

where x_α is the molar concentration of component α in the liquid phase. The temperature and entropy of melting of the end-members (Figure 5) are from the present study for $CaSiO_3$ and our previous study for $MgSiO_3$ (de Koker & Stixrude, 2009). By setting $T_{Mg} = T_{Ca}$, we find the eutectic temperature T_E and composition $x_E = x_{Ca} = 1 - x_{Mg}$. At 25 GPa, we find $x_E = 0.19$ and $T_E = 2820$ K. A recent experimental study (Nomura et al., 2017) also found that the eutectic composition at 24 GPa was shifted substantially toward the $MgSiO_3$ end-member. At the pressure of the core-mantle boundary, we find $x_E = 0.26$ and $T_E = 4900$ K. The eutectic temperature that we find yields an upper bound on the solidus of the multicomponent mantle, consistent with experimental determination of the solidus temperature of peridotite at 4100 K (Fiquet et al., 2010).

Partial melts at the core-mantle boundary are likely to be denser than coexisitng bridgmanite and may be denser than $CaSiO_3$ perovskite, thus supporting the notion that ultralow velocity zones may be related to the accumulation of partial melt at the base of the mantle (Stixrude & Karki, 2005; Williams & Garnero, 1996; Figure 6). We assume a metasilicate melt composition with Ca/(Ca+Mg) equal to the eutectic composition found above and Fe/(Fe + Mg) ratio computed from the bridgmanite-liquid Mg-Fe partition coefficient $K_D = x^C_{Fe}x^L_{Mg}/(x^L_{Fe}x^C_{Mg})$, where superscripts refer to the respective phases liquid (L) and crystal (C), $P = 135.8$ GPa, and $T = 4000$ K. The volumes of all crystalline end-members are from HeFESTo (Stixrude & Lithgow-Bertelloni, 2011). The volumes of the liquid end-members are taken from the present study, our previous study of $MgSiO_3$ (de Koker & Stixrude, 2009), and our determination of the partial molar volumes of FeO and SiO_2 (Ramo & Stixrude, 2014). For Fe concentrations typical of peridotite, the liquid is denser than bridgmanite and may be denser than Ca-perovskite depending on the value of K_D within present uncertainties. For the greater Fe concentration typical of oceanic crust, the liquid is denser than all coexisitng mantle silicates (ferropericlase, the densest crystalline phase over most of the Fe concentration range explored, is not stable in oceanic crustal compositions).

A number of first principles methods now exist for determining the change in melting temperature with pressure or composition, once the melting temperature at one point is known, such as Clausius-Clapeyron integration, determination of solution properties, or Kirkwood-Buff analysis (de Koker et al., 2013; Stixrude & Karki, 2005; Zhou & Miller, 1997). The challenge has been to determine the absolute melting temperature at a given point in pressure or compositional space. The absolute melting temperature of mantle silicates has not before been determined ab initio. We have shown that the ZW method provides a reliable and reasonably efficient means of determining the absolute melting temperature and that the results are internally accurate, within the framework of density functional theory, by comparing with Clausius-Clapeyron integration. We envision the method being applied to other mantle phases, thus providing fundamental constraints on the chemical potentials of end-members in multicomponent liquids and melting processes.

Acknowledgments
This project is supported by the European Research Council under Advanced Grant 291432 MoltenEarth (FP7). Calculations were carried out using the IRIDIS cluster partly owned by University College London, ARCHER of the UK national high-performance computing service, and MARENOSTRUM at the Barcelona Supercomputing Center, Spain, of the PRACE Consortium. Data supporting the conclusions of this paper are found in the text, figures, and supporting information.

References

Alfe, D., Cazorla, C., & Gillan, M. J. (2011). The kinetics of homogeneous melting beyond the limit of superheating. *Journal of Chemical Physics*, *135*(2), 8.

Andrault, D., Petitgirard, S., Nigro, G. L., Devidal, J. L., Veronesi, G., Garbarino, G., & Mezouar, M. (2012). Solid-liquid iron partitioning in Earth's deep mantle. *Nature*, *487*(7407), 354–357.

Bajgain, S. K., Ghosh, D. B., & Karki, B. B. (2015). First-principles simulations of CaO and $CaSiO_3$ liquids: Structure, thermodynamics and diffusion. *Physics and Chemistry of Minerals*, *42*(5), 393–404.

Belonoshko, A. B., Isaev, E. I., Skorodumova, N. V., & Johansson, B. (2006). Stability of the body-centered-tetragonal phase of Fe at high pressure: Ground-state energies, phonon spectra, and molecular dynamics simulations. *Physical Review B*, *74*, 214102.

Boehler, R., Ross, M., & Boercker, D. B. (1996). High-pressure melting curves of alkali halides. *Physical Review B*, *53*, 556–563.

Callen, H. B. (1960). *Thermodynamics*. New York: John Wiley and Sons.
Corgne, A., Liebske, C., Wood, B. J., Rubie, D. C., & Frost, D. J. (2005). Silicate perovskite-melt partitioning of trace elements and geochemical signature of a deep perovskitic reservoir. *Geochimica et Cosmochimica Acta*, *69*(2), 485–496.
Daeges, J., Gleiter, H., & Perepezko, J. H. (1986). Superheating of metal crystals. *Physics Letters A*, *119*(2), 79–82.
de Koker, N., Karki, B. B., & Stixrude, L. (2013). Thermodynamics of the MgO-SiO_2 liquid system in Earth's lowermost mantle from first principles. *Earth and Planetary Science Letters*, *361*, 58–63.
de Koker, N., & Stixrude, L. (2009). Self-consistent thermodynamic description of silicate liquids, with application to shock melting of MgO periclase and $MgSiO_3$ perovskite. *Geophysical Journal International*, *178*(1), 162–179.
Fiquet, G., Auzende, A. L., Siebert, J., Corgne, A., Bureau, H., Ozawa, H., & Garbarino, G. (2010). Melting of peridotite to 140 gigapascals. *Science*, *329*(5998), 1516–1518.
Gasparik, T., Wolf, K., & Smith, C. M. (1994). Experimental-determination of phase-relations in the $CaSiO_3$ system from 8 to 15 GPa. *American Mineralogist*, *79*(11-12), 1219–1222.
Gonzalez-Cataldo, F., Davis, S., & Gutierrez, G. (2016). Melting curve of SiO_2 at multimegabar pressures: Implications for gas giants and super-earths. *Scientific Reports*, *6*, 7.
Hoover, W. G. (1985). Canonical dynamics—Equilibrium phase-space distributions. *Physical Review A*, *31*(3), 1695–1697.
Hoover, W. G., & Ross, M. (1971). Statistical theories of melting. *Contemporary Physics*, *12*(4), 339–356.
Kechin, V. V. (2002). Melting curve equations at high pressure. *Physical Review B*, *65*(5), 052102.
Kresse, G., & Furthmuller, J. (1996). Efficiency of ab-initio total energy calculations for metals and semiconductors using a plane-wave basis set. *Computational Materials Science*, *6*(1), 15–50.
Kresse, G., & Joubert, D. (1999). From ultrasoft pseudopotentials to the projector augmented-wave method. *Physical Review B*, *59*(3), 1758–1775.
Mermin, N. D. (1965). Thermal properties of the inhomogeneous electron gas. *Physical Review*, *137*(5A), A1441–A1443.
Mo, M. Z., Chen, Z., Li, R. K., Dunning, M., Witte, B. B. L., Baldwin, J. K., et al. (2018). Heterogeneous to homogeneous melting transition visualized with ultrafast electron diffraction. *Science*, *360*(6396), 1451–1454.
Nomura, R., Zhou, Y., & Irifune, T. (2017). Melting phase relations in the $MgSiO_3$-$CaSiO_3$ system at 24 GPa. *Progress in Earth and Planetary Science*, *4*, 11.
Perdew, J. P., Ruzsinszky, A., Csonka, G. I., Vydrov, O. A., Scuseria, G. E., Constantin, L. A., et al. (2008). Restoring the density-gradient expansion for exchange in solids and surfaces. *Physical Review Letters*, *100*(13), 136406.
Ramo, D. M., & Stixrude, L. (2014). Spin crossover in Fe_2SiO_4 liquid at high pressure. *Geophysical Research Letters*, *41*, 4512–4518. https://doi.org/10.1002/2014GL060473
Shen, G. Y., & Lazor, P. (1995). Measurement of melting temperatures of some minerals under lower mantle pressures. *Journal of Geophysical Research*, *100*(B9), 17,699–17,713.
Stebbins, J. F., Carmichael, I. S. E., & Moret, L. K. (1984). Heat-capacities and entropies of silicate liquids and glasses. *Contributions to Mineralogy and Petrology*, *86*(2), 131–148.
Stixrude, L. (2014). Melting in super-earths. *Philosophical Transactions of the Royal Society a-Mathematical Physical and Engineering Sciences*, *372*(2014), 20130076.
Stixrude, L., de Koker, N., Sun, N., Mookherjee, M., & Karki, B. B. (2009). Thermodynamics of silicate liquids in the deep Earth. *Earth and Planetary Science Letters*, *278*(3-4), 226–232.
Stixrude, L., & Karki, B. (2005). Structure and freezing of $MgSiO_3$ liquid in Earth's lower mantle. *Science*, *310*(5746), 297–299.
Stixrude, L., & Lithgow-Bertelloni, C. (2011). Thermodynamics of mantle minerals—II. Phase equilibria. *Geophysical Journal International*, *184*(3), 1180–1213.
Stixrude, L., Lithgow-Bertelloni, C., Kiefer, B., & Fumagalli, P. (2007). Phase stability and shear softening in $CaSiO_3$ perovskite at high pressure. *Physical Review B*, *75*, 024108.
Sun, N. Y., Mao, Z., Yan, S., Wu, X., Prakapenka, V. B., & Lin, J. F. (2016). Confirming a pyrolitic lower mantle using self-consistent pressure scales and new constraints on $CaSiO_3$ perovskite. *Journal of Geophysical Research: Solid Earth*, *121*, 4876–4894. https://doi.org/10.1002/2016JB013062
Sun, N., Stixrude, L., de Koker, N., & Karki, B. B. (2011). First principles molecular dynamics simulations of diopside liquid at high pressure. *Geochmica et Cosmochimica Acta*, *75*, 3792–3802.
Tateno, S., Hirose, K., & Ohishi, Y. (2014). Melting experiments on peridotite to lowermost mantle conditions. *Journal of Geophysical Research: Solid Earth*, *119*, 4684–4694. https://doi.org/10.1002/2013JB010616
Tateno, S., Hirose, K., Sakata, S., Yonemitsu, K., Ozawa, H., Hirata, T., et al. (2018). Melting phase relations and element partitioning in MORB to lowermost mantle conditions. *Journal of Geophysical Research: Solid Earth*, *123*, 5515–5531. https://doi.org/10.1029/2018JB015790
Tsuchiya, T., & Tsuchiya, J. (2011). Prediction of a hexagonal SiO_2 phase affecting stabilities of $MgSiO_3$ and $CaSiO_3$ at multimegabar pressures. *Proceedings of the National Academy of Sciences of the United States of America*, *108*(4), 1252–1255.
Wentzcovitch, R. M., Martins, J. L., & Allen, P. B. (1992). Energy versus free-energy conservation in 1st-principles molecular-dynamics. *Physical Review B*, *45*(19), 11,372–11,374.
Williams, Q., & Garnero, E. J. (1996). Seismic evidence for partial melt at the base of Earth's mantle. *Science*, *273*, 1528–1530.
Xu, W. B., Lithgow-Bertelloni, C., Stixrude, L., & Ritsema, J. (2008). The effect of bulk composition and temperature on mantle seismic structure. *Earth and Planetary Science Letters*, *275*(1-2), 70–79.
Zerr, A., Serghiou, G., & Boehler, R. (1997). Melting of $CaSiO_3$ perovskite to 430 kbar and first in-situ measurements of lower mantle eutectic temperatures. *Geophysical Research Letters*, *24*, 909–912.
Zhou, Y. H., & Miller, G. H. (1997). Constraints from molecular dynamics on the liquidus and solidus of the lower mantle. *Geochimica et Cosmochimica Acta*, *61*(14), 2957–2976.